

Intrinsic Zeeman Effect in Graphene

Motohiko Ezawa

Department of Physics, University of Tokyo, Hongo 7-3-1, 113-0033, Japan

(Dated: April 14, 2007)

Abstract

The intrinsic Zeeman energy is precisely one half of the cyclotron energy for electrons in graphene. As a result a Landau-level mixing occurs to create the energy spectrum comprised of the $4j$ -fold degenerated zero-energy level and 4-fold degenerated nonzero-energy levels in the j -layer graphene, where $j = 1, 2, 3$ for monolayer, bilayer and trilayer, respectively. The degeneracy manifests itself in the quantum Hall (QH) effect. We study how the degeneracy is removed by the Coulomb interactions. With respect to the zero-energy level, an excitonic gap opens by making a BCS-type condensation of electron-hole pairs at the filling factor $\nu = 0$. It gives birth to the Ising QH ferromagnet at $\nu = \pm 1$ for monolayer, $\nu = \pm 1, \pm 3$ for bilayer, and $\nu = \pm 1, \pm 3, \pm 5$ for trilayer graphene from the zero-energy degeneracy. With respect to the nonzero-energy level, a remarkable consequence is derived that the effective Coulomb potential depends on spins, since a single energy level contains up-spin and down-spin electrons belonging to different Landau levels. The spin-dependent Coulomb interaction leads to the valley polarization at $\nu = \pm 4, \pm 8, \pm 12, \dots$ for monolayer, $\nu = \pm 2, \pm 6, \pm 10, \dots$ for bilayer, and $\nu = \pm 2, \pm 4, \pm 8, \pm 12, \dots$ for trilayer graphene.

I. INTRODUCTION

Recent experiments has established that the charge carriers in graphene are massless Dirac electrons^{1,2,3,4,5}. Dirac electrons have a peculiar property that they have the intrinsic Zeeman energy precisely one half of the cyclotron energy in magnetic field. Consequently a Landau level mixing occurs so that one energy level contains up-spin and down-spin electrons coming from different Landau levels. It has two important consequences; the emergence of the zero-energy state⁶, and the degeneracy of the up-spin and down-spin states for each nonzero-energy level [Fig.1(a)]. The aim of this paper is to explore new phenomena due to this intrinsic Zeeman effect in graphene.

The quantum Hall effect (QHE) in graphene^{1,2,3,4,5} is unconventional. The filling factors form a series [Fig.1(b)],

$$\nu = 0, \pm 1, \pm \mathbf{2}, \pm 4, \pm \mathbf{6}, \pm 8, \pm \mathbf{10}, \pm 12, \dots, \quad (1.1)$$

where the bold-face series had been predicted^{7,8,9} before it was found experimentally^{1,2,3,4}, while the full series was discovered later⁵ with larger magnetic field applied. Subsequently theoretical works^{10,11,12,13,14} have been made to interpret the series. Furthermore, the series reads

$$\nu = 0, \pm 1, \pm 2, \pm 3, \pm \mathbf{4}, \pm 6, \pm \mathbf{8}, \pm 10, \pm \mathbf{12}, \dots, \quad (1.2)$$

in a bilayer graphene, where the bold-face series has been found experimentally⁴ and studied theoretically¹⁵, while it reads

$$\nu = 0, \pm 1, \pm 2, \pm 3, \pm 4, \pm 5, \pm \mathbf{6}, \pm 8, \pm \mathbf{10}, \pm 12, \dots, \quad (1.3)$$

in a trilayer graphene, where the bold-face series has been predicted theoretically¹⁶. In this paper we show that the full series emerge when Coulomb interactions become important. It is notable that the basic height in the Hall conductance is $4e^2/h$ for the bold-face series for all these graphene systems, indicating the 4-fold degeneracy of the energy level except for the first step at the $\nu = 0$ point within noninteracting theory.

Conduction and valence bands in graphene form conically shaped valleys, touching at a point [Fig.2]. There are two inequivalent Brillouin zone corners, called the K and K' points, at which massless Dirac electrons emerge^{17,18,19}. Let us refer to the valley as the Dirac valley, and assign the valley index to the electron so that the electron at the K (K') point carries the index $\tau = + (-)$. As we have mentioned, the graphene QH system is characterized by the emergence of the zero-energy state and the degeneracy of the up-spin and down-spin states for each nonzero-energy level. Since this holds separately at the K and K' points, each energy level has a 4-fold degeneracy [Fig.1(a)], and the noninteracting system has the SU(4) symmetry.

Intriguing phenomena occur when we introduce Coulomb interactions. It is necessary to consider the Coulomb effect in the zero-energy state and nonzero-energy states separately.

The zero-energy state is distinctive, since it contains both electrons and holes. Electron-hole pairs form an excitonic condensation due to attractive interaction, producing an excitonic gap. We obtain a BCS-type state of electron-hole pairs at $\nu = 0$. As a consequence of excitonic condensation, the degeneracy of the zero-energy state is resolved into two subbands each of which contains either electrons or holes. The Coulomb Hamiltonian, projected to each of them, has the U(1) symmetry but is broken into the Z₂ symmetry. We obtain the Ising QH ferromagnet at $\nu = \pm 1$.

We next study nonzero-energy states of electrons, where a single energy level contains up-spin and down-spin electrons belonging to different Landau levels [Fig.1(a)]. We derive a remarkable consequence that the effective Coulomb potential depends on the spin and the valley in each energy

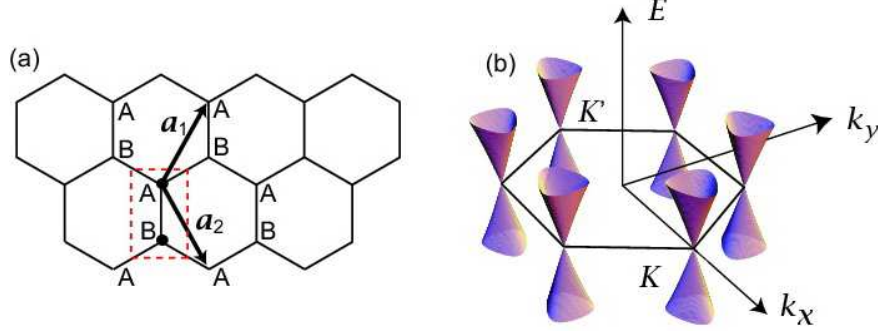


FIG. 2: (Color online) (a) Graphene is made of a honeycomb lattice. It consists of two triangular sublattices generated by the two basis vectors \mathbf{a}_1 and \mathbf{a}_2 from the base points A and B in primitive cell (dotted rectangle). (b) The reciprocal lattice is also a honeycomb lattice. The first Brillouin zone is depicted together with the Dirac valleys describing the low-energy band structure.

II. DIRAC ELECTRONS AND INTRINSIC ZEEMAN EFFECT

A. Dirac Hamiltonian

The low-energy band structure of graphene is described by conically shaped valleys, touching at a point. There exists two inequivalent Brillouin zone corners $\pm \mathbf{K} = (\pm 4\pi/\sqrt{3}a, 0)$ with a the lattice constant. They are called the K and K' points [Fig.2(b)]. The two-dimensional energy dispersion relation is linear in these Dirac valleys,

$$\mathcal{E}_\tau(\mathbf{k}) = \hbar v_F |\mathbf{k} - \tau \mathbf{K}|, \quad (2.1)$$

where v_F is the Fermi velocity, and $\tau = \pm$ is the valley index. This linear behavior has been confirmed experimentally²⁰ up to 3eV. It is convenient to make the change of variable, $\mathbf{k} = \mathbf{k}' + \tau \mathbf{K}$, and rewrite the dispersion relation as

$$\mathcal{E}(\mathbf{k}') = \hbar v_F |\mathbf{k}'|. \quad (2.2)$$

We use the variable \mathbf{k}' to show that $\hbar \mathbf{k}'$ is the relative momentum of electrons, $|\mathbf{k}'| \ll |\mathbf{K}|$, measured from $\tau \mathbf{K}$ at the K or K' point.

There exists one electron per one carbon and the band-filling factor is 1/2 in graphene. Hence we have electron excitations in the conduction band and hole excitations in the valence band. Furthermore there exists the electron-hole symmetry.

The dispersion relation (2.2) is that of ‘relativistic’ Dirac fermions^{17,18,19}. Hence the second-quantized Hamiltonian is given by

$$H = \sum_{\tau=\pm} \int d^2x \Psi_\tau^\dagger(\mathbf{x}) H_D^\tau \Psi_\tau(\mathbf{x}), \quad (2.3)$$

where H_D^τ is the quantum mechanical Hamiltonian,

$$H_D^\tau = v_F (\tau \sigma_x p_x + \sigma_y p_y) \gamma_5, \quad (2.4)$$

with $p_i \equiv -i\hbar\partial_i$, the Pauli matrix σ_i and the Dirac matrix γ_5 . The field $\Psi_\tau(\mathbf{x})$ consists of eight components, corresponding to the spin degree of freedom, the electron-hole degree of freedom and

the valley degree of freedom. Being massless, the Hamiltonian describes Weyl fermions, and the spin index σ represents the helicity.

The field operator $\Psi_\tau(\mathbf{x})$ is expanded in terms of the eigenfunctions of H_D^τ as

$$\Psi_\tau(\mathbf{x}) = \Psi_{e\tau}(\mathbf{x}) + \Psi_{h\tau}(\mathbf{x}), \quad (2.5)$$

with

$$\Psi_{e\tau}(\mathbf{x}) = \sum_\sigma \int \frac{d^2k'}{2\pi} c_\tau^\sigma(\mathbf{k}') u_\sigma^\tau(\mathbf{k}') e^{i\mathbf{k}'\cdot\mathbf{x}}, \quad (2.6a)$$

$$\Psi_{h\tau}(\mathbf{x}) = \sum_\sigma \int \frac{d^2k'}{2\pi} d_\tau^{\sigma\dagger}(\mathbf{k}') v_\sigma^\tau(\mathbf{k}') e^{-i\mathbf{k}'\cdot\mathbf{x}}, \quad (2.6b)$$

where $c_\tau^\sigma(\mathbf{k}')$ and $d_\tau^{\sigma\dagger}(\mathbf{k}')$ are the annihilation operator of an electron and the creation operator of a hole, respectively, while $u_\sigma^\tau(\mathbf{k}')$ and $v_\sigma^\tau(\mathbf{k}')$ are the corresponding eigenfunctions of the Dirac operator (2.4) with the eigenvalue $\mathcal{E}(\mathbf{k}') = \pm \hbar v_F |\mathbf{k}'|$.

The field $\Psi_\tau(\mathbf{x})$ describes solely the dynamics of electrons localized in each Dirac valley at the K or K' point. In the dispersion relation (2.2), $\hbar\mathbf{k}'$ is the momentum fluctuation around $\pm\hbar\mathbf{K}$ at the K or K' point. The total momentum of the electron is not $\hbar\mathbf{k}'$ but $\hbar\mathbf{k} = \hbar\mathbf{k}' \pm \hbar\mathbf{K}$. Due to this fact, the eigenfunctions $u_\sigma^\tau(\mathbf{k}')$ and $v_\sigma^\tau(\mathbf{k}')$ are not wave functions but envelope functions²¹. The wave functions are given by $e^{i\tau\mathbf{K}\cdot\mathbf{x}} u_\sigma^\tau(\mathbf{x})$ and $e^{i\tau\mathbf{K}\cdot\mathbf{x}} v_\sigma^\tau(\mathbf{x})$. Accordingly, the field operators of electrons and holes are

$$\psi_{e\tau}(\mathbf{x}) = e^{i\tau\mathbf{K}\cdot\mathbf{x}} \Psi_{e\tau}(\mathbf{x}), \quad \psi_{h\tau}(\mathbf{x}) = e^{i\tau\mathbf{K}\cdot\mathbf{x}} \Psi_{h\tau}(\mathbf{x}). \quad (2.7)$$

Thus, to analyze the Coulomb interaction, it is necessary to use $\psi_{e\tau}(\mathbf{x})$ and $\psi_{h\tau}(\mathbf{x})$. In Appendix A we derive the Dirac Hamiltonian (2.4) based on the effective-mass description²¹.

We make a comment on the factor τ in front of σ_x in (2.4). It has the standard expression of the Dirac Hamiltonian for $\tau = +$, that is, at the K point. The K point is transformed into the K' point under the mirror reflection. Corresponding to this we have the mirror-reflected Dirac Hamiltonian (2.4) for $\tau = -$, that is, at the K' point. The total Hamiltonian (2.3) has the mirror symmetry.

B. Landau Levels

We apply the magnetic field to a graphene sheet taken on the xy plane. It is introduced to the Hamiltonian (2.3) by making the minimal substitution,

$$H_D^\tau = v_F (\tau \sigma_x P_x + \sigma_y P_y) \gamma_5, \quad (2.8)$$

where $P_i \equiv -i\hbar\partial_i + eA_i$ is the covariant momentum. We assume a homogeneous magnetic field $\mathbf{B} = \nabla \times \mathbf{A} = (0, 0, -B)$ with $B > 0$ along the z axis. The presence of the external magnetic field modifies the mirror symmetry as follows: The modified mirror reflection not only transforms the K point into the K' point but also reverses the direction of the magnetic field to maintain the symmetry. This is most clearly seen in (2.19), as we shall discuss later. Consequently, the K and K' points become physically distinguishable.

Electrons make cyclotron motion in magnetic field. The helicity is no longer a good variable, since there exists a special direction for the spin, that is, the direction of magnetic field. In this

case it is convenient to use the standard representation for the Dirac matrices, where

$$\gamma_5 = \begin{pmatrix} 0 & 1 \\ 1 & 0 \end{pmatrix}. \quad (2.9)$$

In order to discuss the QHE, we solve the quantum mechanical problem with the Hamiltonian (2.8) in each Dirac valley,

$$H_D^\tau \Psi_\tau(\mathbf{x}) = \mathcal{E}_\tau \Psi_\tau(\mathbf{x}), \quad (2.10)$$

and we expand the field operator in terms of the new eigenfunctions.

To solve the eigen equation (2.10) we express the Hamiltonian (2.8) as

$$H_D^\tau = \begin{pmatrix} 0 & Q_\tau \\ Q_\tau & 0 \end{pmatrix}, \quad (2.11)$$

with the use of (2.9) for γ_5 , where

$$Q_\tau = v_F (\tau \sigma_x P_x + \sigma_y P_y). \quad (2.12)$$

It is diagonalized as

$$H_D^\tau = \text{diag.} \left(\sqrt{Q_\tau Q_\tau}, -\sqrt{Q_\tau Q_\tau} \right). \quad (2.13)$$

We introduce a pair of operators

$$a = \frac{\ell_B(P_x + iP_y)}{\sqrt{2}\hbar}, \quad a^\dagger = \frac{\ell_B(P_x - iP_y)}{\sqrt{2}\hbar}, \quad (2.14)$$

satisfying $[a, a^\dagger] = 1$, where $\ell_B = \sqrt{\hbar/eB}$ is the magnetic length. Since the operators (2.12) is rewritten as

$$Q_+ = \hbar\omega_c \begin{pmatrix} 0 & a^\dagger \\ a & 0 \end{pmatrix}, \quad Q_- = \hbar\omega_c \begin{pmatrix} 0 & a \\ a^\dagger & 0 \end{pmatrix}, \quad (2.15)$$

with $\omega_c = \sqrt{2}\hbar v_F/\ell_B$, the diagonalized Hamiltonian reads

$$H_D^+ = \hbar\omega_c \text{diag.} \left(\sqrt{a^\dagger a}, \sqrt{a a^\dagger}, -\sqrt{a^\dagger a}, -\sqrt{a a^\dagger} \right), \quad (2.16a)$$

$$H_D^- = \hbar\omega_c \text{diag.} \left(\sqrt{a a^\dagger}, \sqrt{a^\dagger a}, -\sqrt{a a^\dagger}, -\sqrt{a^\dagger a} \right). \quad (2.16b)$$

Since $a^\dagger a$ is the number operator, the eigenvalue of the Dirac Hamiltonian H_D^\pm follows immediately,

$$\mathcal{E}_N^+ = \hbar\omega_c \left(\sqrt{N}, \sqrt{N+1}, -\sqrt{N}, -\sqrt{N+1} \right), \quad (2.17a)$$

$$\mathcal{E}_N^- = \hbar\omega_c \left(\sqrt{N+1}, \sqrt{N}, -\sqrt{N+1}, -\sqrt{N} \right), \quad (2.17b)$$

with the eigenstate

$$|N\rangle = \frac{1}{\sqrt{N!}}(a^\dagger)^N|0\rangle, \quad (2.18)$$

where $N = 0, 1, 2, 3, \dots$.

The operators a and a^\dagger are the Landau-level ladder operators. Hence, N in (2.17) represents the Landau-level index. We have found that the energy of an electron in the N th Landau level is either $\hbar\omega_c\sqrt{N}$ or $\hbar\omega_c\sqrt{N+1}$. It is curious that the energy of an electron in the lowest Landau level ($N=0$) is zero though it performs cyclotron motion. This puzzle is solved in the succeeding subsection.

C. Pauli Hamiltonian

To reveal the intrinsic structure of the energy spectrum, we investigate the Hamiltonian^{14,22,23,24}

$$H_P^\pm = Q_\pm Q_\pm = v_F^2 \left[(-i\hbar\nabla + e\mathbf{A})^2 \mp e\hbar\sigma_z B \right], \quad (2.19)$$

which is the building blocks of the Dirac Hamiltonian (2.13). Here, the direction of the magnetic field is found to be effectively opposite at the K and K' points. Since this has the same form as the Pauli Hamiltonian with the mass $m^* = 1/4v_F^2$ except for the dimension, we call it the Pauli Hamiltonian for brevity. The salient feature of the *relativistic* Dirac Hamiltonian is that its spectrum is mapped from that of the *nonrelativistic* Pauli Hamiltonian. Thus, the energy eigenvalue \mathcal{E}_N^τ of the Dirac Hamiltonian H_D^τ is constructed as $\mathcal{E}_N^\tau = \pm\sqrt{E_N^\tau}$ from the energy eigenvalue E_N^τ of the Pauli Hamiltonian H_P^τ .

In the Pauli Hamiltonian (2.19), the first term is the kinetic term while the second term is the Zeeman term. It is fixed uniquely as an intrinsic property of the Dirac theory: We call it the intrinsic Zeeman effect.

The Landau level is created by electrons making cyclotron motion. In the conventional QHE, since the Zeeman energy can be considered much smaller than the Landau-level separation, we may treat it as a perturbation. However, this is not the case in graphene. According to the Pauli Hamiltonian (2.19), the intrinsic Zeeman energy is precisely one half of the cyclotron energy for Dirac electrons, and two Landau levels mix to create one energy level, as illustrated in Fig.1(a).

We consider the K point ($\tau = +$). It is obvious that the up-spin and down-spin states are eigenstates of the Pauli Hamiltonian (2.19) and hence eigenstates of the Dirac Hamiltonian (2.13), and that the up-spin state has a lower energy than the down-spin state when they belong to the same Landau level. On the other hand, the direction of the spin is opposite at the K and K' points. Hence, we can make the following identification of quantum numbers for electrons in the N th level ($N \geq 1$) of the energy spectrum [Fig.1(a)],

$$\mathcal{E}_N^{+\uparrow} = \mathcal{E}_{N-1}^{+\downarrow} = \mathcal{E}_N^{-\downarrow} = \mathcal{E}_{N-1}^{-\uparrow} = \hbar\omega_c\sqrt{N}. \quad (2.20)$$

A similar identification can be made for holes in the N th energy level ($N \geq 1$). The zeroth energy level ($N=0$) consists of the up-spin electron and the down-spin hole at the K point, and the down-spin electron and the up-spin hole at the K' point [Fig.1(a)], coming from the lowest Landau levels for electrons and holes.

Counting the states at the K and K' points all together, one energy level has a 4-fold degeneracy. Each filled energy level contributes one conductance quantum e^2/\hbar to the Hall conductivity. Consequently the resulting series is $\nu = \pm 2, \pm 6, \pm 10, \dots$, which accounts for the bold-face series (1.1) in the monolayer graphene.

D. Field Operators

We focus on electrons in the N th energy level. (Essentially the same analysis is applicable to holes.) We start with the quantum-mechanical state in a single Landau level. We decompose the electron coordinate $\mathbf{x} = (x, y)$ into the guiding center $\mathbf{X} = (X, Y)$ and the relative coordinate $\mathbf{R} = (R_x, R_y)$, $\mathbf{x} = \mathbf{X} + \mathbf{R}$, where $R_x = -P_y/eB$ and $R_y = P_x/eB$ with $\mathbf{P} = (P_x, P_y)$ the covariant momentum. They satisfy the commutation relations $[X, Y] = -i\ell_B^2$, $[P_x, P_y] = i\hbar^2/\ell_B^2$, $[X, P_x] = [X, P_y] = [Y, P_x] = [Y, P_y] = 0$. We define a set of operators b, b^\dagger by

$$b = \frac{1}{\sqrt{2}\ell_B}(X - iY), \quad b^\dagger = \frac{1}{\sqrt{2}\ell_B}(X + iY), \quad (2.21)$$

obeying $[b, b^\dagger] = 1$, in addition to a set of operators a, a^\dagger by (2.14). The quantum-mechanical states are the Fock states,

$$|N, n\rangle = \frac{1}{\sqrt{N!n!}}(a^\dagger)^N(b^\dagger)^n|0\rangle \quad (2.22)$$

with $|0\rangle$ the Fock vacuum, $a|0\rangle = b|0\rangle = 0$.

We have constructed the energy spectrum of the Dirac Hamiltonian (2.13) in each Dirac valley, as illustrated in Fig.1(a). The N th energy level ($N \neq 0$) contains electrons coming from two Dirac valleys ($\tau = \pm$), whose field operators are expanded in terms of the eigenfunctions. Corresponding to $\mathcal{E}_N^{+\uparrow}, \mathcal{E}_{N-1}^{+\downarrow}, \mathcal{E}_N^{-\downarrow}$ and $\mathcal{E}_{N-1}^{-\uparrow}$ in (2.20), we have

$$\psi_{N+}^\uparrow(\mathbf{x}) = e^{i\mathbf{K}\mathbf{x}} \sum_n \langle \mathbf{x} | N, n \rangle c_+^\uparrow(N, n), \quad (2.23a)$$

$$\psi_{N-}^\downarrow(\mathbf{x}) = e^{-i\mathbf{K}\mathbf{x}} \sum_n \langle \mathbf{x} | N, n \rangle c_-^\downarrow(N, n), \quad (2.23b)$$

$$\psi_{N+}^\downarrow(\mathbf{x}) = e^{i\mathbf{K}\mathbf{x}} \sum_n \langle \mathbf{x} | N-1, n \rangle c_+^\downarrow(N-1, n), \quad (2.23c)$$

$$\psi_{N-}^\uparrow(\mathbf{x}) = e^{-i\mathbf{K}\mathbf{x}} \sum_n \langle \mathbf{x} | N-1, n \rangle c_-^\uparrow(N-1, n), \quad (2.23d)$$

where $c_\tau^\sigma(N, n)$ is the annihilation operator acting on the Fock state $|N, n\rangle$ at the τ point. In what follows we suppress the Landau-level index N in $c_\tau^\sigma(N, n)$ with the understanding that $c_+^\uparrow(n) = c_+^\uparrow(N, n)$, $c_-^\downarrow(n) = c_-^\downarrow(N, n)$, $c_+^\downarrow(n) = c_+^\downarrow(N-1, n)$, $c_-^\uparrow(n) = c_-^\uparrow(N-1, n)$. See (2.7) with respect to the factor $e^{\pm i\mathbf{K}\mathbf{x}}$. The electron operators in the zeroth energy level are given by $\psi_{N+}^\uparrow(\mathbf{x})$ and $\psi_{N-}^\downarrow(\mathbf{x})$ with $N = 0$.

III. COULOMB INTERACTIONS

We make the basic assumption that the cyclotron energy is much larger than the Coulomb energy as in the conventional QHE^{25,26,27}. We neglect the Landau-level mixing by the Coulomb interaction, and analyze it within one energy level [Fig.1(a)]. There exists a consistent formalism, known as the Landau-level projection. The projected theory presents not only a good approximation but also an essential way to reveal a new physics inherent to the QH system^{25,26,27}. Then we may treat the electron system, the hole system and the zero-energy system independently of each other. The hole system has the same structure as the electron system due to the electron-hole symmetry. On

the other hand, the zero-energy system contains both electrons and holes. We study the electron system in this section, and the zero-energy system of electrons and holes in Section IV.

Assuming all lower levels are filled up, we study the Coulomb interaction between electrons confined within the N th energy level ($N \geq 1$). The Coulomb Hamiltonian reads

$$H = \frac{1}{2} \int \int d^2x d^2y V(\mathbf{x} - \mathbf{y}) \rho(\mathbf{x}) \rho(\mathbf{y}), \quad (3.24)$$

where $\rho(\mathbf{x})$ is the density operator

$$\rho(\mathbf{x}) = \sum_{\tau\tau'\sigma} \psi_{\tau}^{\sigma\dagger}(\mathbf{x}) \psi_{\tau'}^{\sigma}(\mathbf{x}). \quad (3.25)$$

The Landau-level projection of the Coulomb Hamiltonian (3.24) is a simple generalization of the lowest-Landau-level projection²⁸ familiar in the conventional QHE. We require the density operator to be comprised solely of the electron fields belonging to the N th energy level. Thus, from (3.25) we construct the projected density operator $\rho_N(\mathbf{x})$ by

$$\rho_N(\mathbf{x}) = \sum_{\tau\tau'\sigma} \psi_{N\tau}^{\sigma\dagger}(\mathbf{x}) \psi_{N\tau'}^{\sigma}(\mathbf{x}), \quad (3.26)$$

where $\psi_{N\tau}^{\sigma}(\mathbf{x})$ is the field operator (2.23). As we show in Appendix II, the projected density operator is rewritten in the momentum space as

$$\rho_N(\mathbf{q}) = \sum_{\tau\tau'\sigma} F_{\tau\tau'}^{\sigma}(\mathbf{q}) \hat{D}_{\tau\tau'}^{\sigma\sigma}(\mathbf{q}), \quad (3.27)$$

where $\hat{D}_{\tau\tau'}^{\sigma\sigma'}(\mathbf{q})$ is the bare density operator²⁹,

$$\hat{D}_{\tau\tau'}^{\sigma\sigma'}(\mathbf{q}) = \frac{1}{2\pi} \sum_{mn} \langle m | e^{-i[\mathbf{q} + \tau\mathbf{K} - \tau'\mathbf{K}]\mathbf{X}} | n \rangle c_{\tau}^{\sigma\dagger}(m) c_{\tau'}^{\sigma'}(n), \quad (3.28)$$

and $F_{\tau\tau'}^{\sigma}(\mathbf{q})$ is the form factor,

$$F_{++}^{\uparrow}(\mathbf{q}) = F_{--}^{\downarrow}(\mathbf{q}) = F_N(\mathbf{q}), \quad (3.29a)$$

$$F_{++}^{\downarrow}(\mathbf{q}) = F_{--}^{\uparrow}(\mathbf{q}) = F_{N-1}(\mathbf{q}), \quad (3.29b)$$

$$F_{+-}^{\uparrow}(\mathbf{q}) = F_{-+}^{\downarrow}(\mathbf{q}) = G_N(\mathbf{q}), \quad (3.29c)$$

$$F_{-+}^{\uparrow}(\mathbf{q}) = F_{+-}^{\downarrow}(\mathbf{q}) = G_N^*(-\mathbf{q}), \quad (3.29d)$$

with

$$F_N(\mathbf{q}) = \langle N | e^{-i\mathbf{q}\mathbf{R}} | N \rangle, \quad (3.30a)$$

$$G_N(\mathbf{q}) = \langle N | e^{-i(\mathbf{q} - \mathbf{K})\mathbf{R}} | N - 1 \rangle. \quad (3.30b)$$

Here we have used the relation, $\mathbf{q} = \mathbf{q} + 3\mathbf{K}$, due to the lattice structure. It should be remarked that the bare density operator $\hat{D}_{\tau\tau'}^{\sigma\sigma'}(\mathbf{q})$ involves only the guiding center coordinate \mathbf{X} , while the form factor $F_{\tau\tau'}^{\sigma}(\mathbf{q})$ involves only the relative coordinate \mathbf{R} .

The form factors are explicitly given by using³⁰

$$\langle N+M | e^{i\mathbf{q}\mathbf{R}} | N \rangle = \frac{\sqrt{N!}}{\sqrt{(N+M)!}} \left(\frac{\ell_B \mathbf{q}}{\sqrt{2}} \right)^M L_N^M \left(\frac{\ell_B^2 \mathbf{q}^2}{2} \right) e^{-\frac{1}{4}\ell_B^2 \mathbf{q}^2}$$

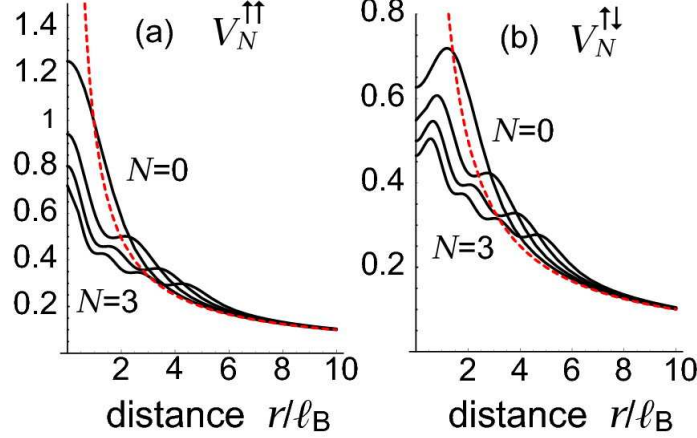


FIG. 3: (Color online) The spin dependence of the effective Coulomb potential. The vertical axis is the potential in unit of $e^2/4\pi\epsilon\ell_B$. The horizontal axis is the distance r in unit of ℓ_B . The dotted red curve represents the ordinary Coulomb potential without the form factor. (a) The effective Coulomb potential $V_N^{\uparrow\uparrow}(r)$ in the N th energy level for $N = 0, 1, 2, 3$ from top to bottom. Note that $V_N^{\downarrow\downarrow}(r) = V_{N-1}^{\uparrow\uparrow}(r)$. It describes interactions between electrons with the same spin. (b) The effective Coulomb potential $V_N^{\uparrow\downarrow}(r)$ for $N = 0, 1, 2, 3$ from top to bottom. It describes interactions between electrons with the different spins.

for $M \geq 0$ in terms of associated Laguerre polynomials.

A comment is in order on the form factors. It is easy to see that¹²

$$G_N(\mathbf{q}) \simeq e^{-\frac{1}{2}\ell_B^2|\mathbf{K}|^2} F_N(\mathbf{q}). \quad (3.31)$$

Thus, $G_N(\mathbf{q})$ is exponentially smaller than $F_N(\mathbf{q})$. For instance, $F_{+-}^{\uparrow}(\mathbf{q}) \equiv G_N(\mathbf{q})$ represents the transfer of the up-spin electron ($\sigma = \uparrow$) from the K' point ($\tau = -$) to the K point ($\tau = +$). Hence, such a mixing between the K and K' points is actually negligible.

The projected Coulomb Hamiltonian is constructed by substituting the projected density (3.27) into the Hamiltonian (3.24),

$$\begin{aligned} H_N &= \pi \int d^2q V(\mathbf{q}) \rho_N(-\mathbf{q}) \rho_N(\mathbf{q}) \\ &= \pi \sum_{\tau\tau'\sigma'} \sum_{\lambda\lambda'\sigma'} \int d^2q V_{N;\tau\tau'\lambda\lambda'}^{\sigma\sigma'}(\mathbf{q}) \hat{D}_{\tau\tau'}^{\sigma}(-\mathbf{q}) \hat{D}_{\lambda\lambda'}^{\sigma'}(\mathbf{q}), \end{aligned} \quad (3.32)$$

where $V_{N;\tau\tau'\lambda\lambda'}^{\sigma\sigma'}(\mathbf{q})$ is the effective Coulomb potential in the N th energy level,

$$V_{N;\tau\tau'\lambda\lambda'}^{\sigma\sigma'}(\mathbf{q}) = V(\mathbf{q}) F_{\tau\tau'}^{\sigma}(-\mathbf{q}) F_{\lambda\lambda'}^{\sigma'}(\mathbf{q}) \quad (3.33)$$

with

$$V(\mathbf{q}) = \frac{e^2}{4\pi\epsilon|\mathbf{q}|}. \quad (3.34)$$

It is remarkable that the effective Coulomb potential depends on the spin and the valley through the form factors $F_{\tau\tau'}^{\sigma}(\mathbf{q})$ characterizing Landau levels.

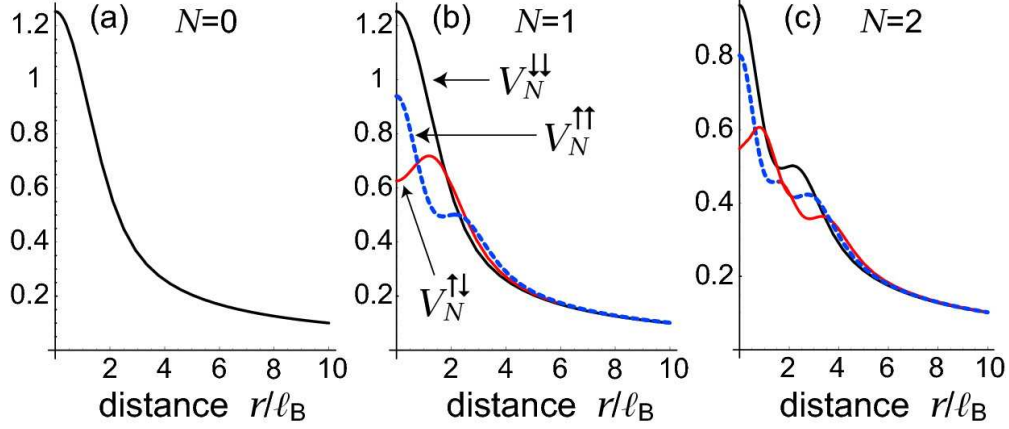


FIG. 4: (Color online) The spin dependence of the effective Coulomb potential $V_N^{\uparrow\downarrow}(r)$, $V_N^{\uparrow\uparrow}(r)$ and $V_N^{\downarrow\downarrow}(r)$ in the N th energy level for (a) $N = 0$, (b) $N = 1$, and (c) $N = 2$. All effective potentials agree for the lowest energy level ($N = 0$). The vertical axis is the potential in unit of $e^2/4\pi\epsilon\ell_B$.

The typical effective Coulomb potentials in the N th energy level at the K point are

$$V_N^{\uparrow\uparrow}(\mathbf{q}) = V(\mathbf{q})F_N(-\mathbf{q})F_N(\mathbf{q}), \quad (3.35a)$$

$$V_N^{\downarrow\downarrow}(\mathbf{q}) = V(\mathbf{q})F_{N-1}(-\mathbf{q})F_{N-1}(\mathbf{q}), \quad (3.35b)$$

$$V_N^{\uparrow\downarrow}(\mathbf{q}) = V(\mathbf{q})F_N(-\mathbf{q})F_{N-1}(\mathbf{q}). \quad (3.35c)$$

The potential $V_N^{\sigma\sigma}(\mathbf{q})$ stands for the interaction between electrons with the same spin σ , $V_N^{\uparrow\downarrow}(\mathbf{q})$ for the interaction between electrons with the different spin. The spin direction is reversed at the K' point. We have illustrated the effective Coulomb potentials in Figs.3 and 4.

We note that the effective potential $V_N^{\uparrow\uparrow}(\mathbf{q})$ for electrons with the same spin in the N th energy level has precisely the same form as in the standard QHE for electrons in the N th Landau level: Compare Fig.3(a) with Fig.7 in Ref.³¹. On the other hand the effective potential $V_N^{\uparrow\downarrow}(\mathbf{q})$ for electrons with the different spins are entirely new.

IV. EXCITONIC CONDENSATION

It is necessary to pay a special attention to the zero-energy level ($N = 0$), since it contains both electrons and holes. Let us recapture the properties of the zero-energy level [Fig.5]. In the absence of the magnetic field the band structure is given by the Dirac valleys associated with the dispersion relation (2.2), as illustrated in Fig.5(a). When the magnetic field is applied, the band structure is changed to generate Landau levels [Fig.5(b)]. However, the Dirac electron is subject to the intrinsic Zeeman effect, which induces a Landau-level mixing, and the zero-energy state emerges for up-spin electrons as well as down-spin holes [Fig.5(c)]. There exists an attractive Coulomb force between an electron and a hole. Hence we expect them to make an excitonic condensation, producing a gap to the electron and hole states [Fig.5(d)].

The excitonic condensation in graphene has been studied in various contexts^{13,32,33,34}. Here, we present a clear-cut approach to this problem on the analogy of the BCS theory. Our physical picture is summarized in Fig.5. The remarkable point is that the kinetic term is quenched in each

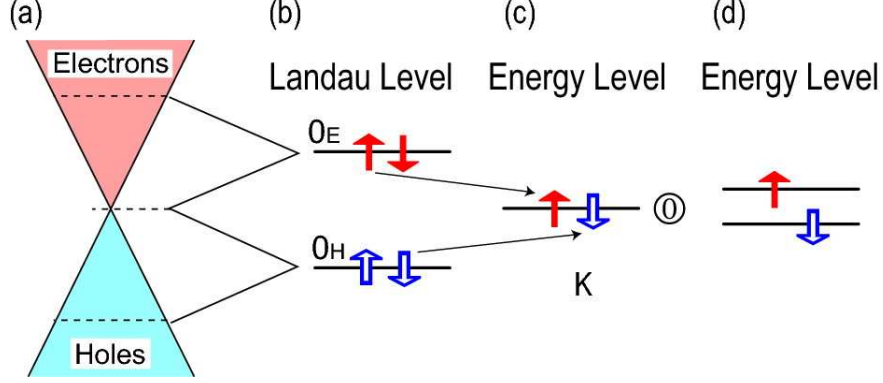


FIG. 5: (Color online) (a) Electron states (blue region) and hole states (red region) in the Dirac valley at the K point. (b) When the magnetic field is applied, the band structure is changed to generate Landau levels. (c) The intrinsic Zeeman effect induces a Landau-level mixing, and the zero-energy state with the up-spin electron and the down-spin hole emerges. (d) They make an excitonic condensation to form a BCS-type state, producing a gap to the electron and hole states.

Landau level, and hence it is also absent in the zero-energy level. This simplifies considerably our analysis.

The field operators present in the zero-energy level are $\psi_{e+}^\dagger(\mathbf{x})$, $\psi_{e-}^\dagger(\mathbf{x})$ for electrons and $\psi_{h+}^\dagger(\mathbf{x})$, $\psi_{h-}^\dagger(\mathbf{x})$ for holes coming from the $N = 0$ Landau levels [Fig.1(a)]. It is sufficient to investigate electron-hole pairs at the K and K' points separately. An exciton composed of an electron and a hole belonging to different valleys is fragile, because their effective Coulomb potential involves the factor $e^{-\frac{1}{2}\ell_B^2|\mathbf{K}|^2}$ compared with the one within the K point: See (3.29) and (3.31). For definiteness, we consider the K point [Fig.5].

The effective Coulomb potential (3.33) is simple in the lowest Landau level,

$$V^{\text{eff}}(\mathbf{q}) = V(\mathbf{q})e^{-\ell_B^2\mathbf{q}^2/2}. \quad (4.36)$$

We consider the effective Hamiltonian together with this effective potential,

$$H^{\text{eff}} = - \int d^2x d^2y V^{\text{eff}}(\mathbf{x} - \mathbf{y}) \psi_e^{\dagger\uparrow}(\mathbf{x}) \psi_e^{\dagger}(\mathbf{x}) \psi_h^{\dagger\downarrow}(\mathbf{y}) \psi_h^{\dagger}(\mathbf{y}), \quad (4.37)$$

where $\psi_e^{\dagger\uparrow}(\mathbf{x})$ and $\psi_h^{\dagger\downarrow}(\mathbf{x})$ are the up-spin electron field and the down-spin hole field, respectively. The Hamiltonian is rewritten as

$$H^{\text{eff}} = -\pi \int V^{\text{eff}}(\mathbf{q}) \psi_e^{\dagger\uparrow}(\mathbf{k} + \mathbf{q}) \psi_h^{\dagger\downarrow}(\mathbf{k}') \psi_h^{\dagger}(\mathbf{k}' - \mathbf{q}) \psi_e^{\dagger}(\mathbf{k}). \quad (4.38)$$

Here and here after, under the symbol \int , the integration over momentum variables is understood.

We derive the gap equation, following the analysis familiar in the BCS theory. We take the terms satisfying $\mathbf{q} = \mathbf{k}' - \mathbf{k}$ as the dominant ones, and approximate the Hamiltonian as

$$H^{\text{eff}} \simeq -\pi \int V^{\text{eff}}(\mathbf{k}' - \mathbf{k}) \psi_e^{\dagger\uparrow}(\mathbf{k}') \psi_h^{\dagger\downarrow}(\mathbf{k}') \psi_h^{\dagger}(\mathbf{k}) \psi_e^{\dagger}(\mathbf{k}). \quad (4.39)$$

We define the singlet excitonic gap function by

$$\Delta(\mathbf{k}) = \int d^2k' V^{\text{eff}}(\mathbf{k}' - \mathbf{k}) \langle \psi_e^{\dagger\uparrow}(\mathbf{k}') \psi_h^{\dagger\downarrow}(\mathbf{k}') \rangle, \quad (4.40)$$

which can be taken to be positive without loss of generality.

The mean-field Hamiltonian reads

$$H^{\text{eff}} \simeq -\pi \int [\Delta(\mathbf{k}) \psi_{\text{h}}^{\dagger}(\mathbf{k}) \psi_{\text{e}}^{\dagger}(\mathbf{k}) + \psi_{\text{e}}^{\dagger}(\mathbf{k}) \psi_{\text{h}}^{\dagger}(\mathbf{k}) \Delta^*(\mathbf{k})]. \quad (4.41)$$

By setting

$$\Psi_1(\mathbf{k}) = \frac{1}{\sqrt{2}} [\psi_{\text{e}}^{\dagger}(\mathbf{k}) + \psi_{\text{h}}^{\dagger}(\mathbf{k})], \quad (4.42\text{a})$$

$$\Psi_2(\mathbf{k}) = \frac{1}{\sqrt{2}} [\psi_{\text{e}}^{\dagger}(\mathbf{k}) - \psi_{\text{h}}^{\dagger}(\mathbf{k})], \quad (4.42\text{b})$$

it is easy to diagonalize (4.41) as

$$H^{\text{eff}} \simeq \pi \int d^2k \Delta(\mathbf{k}) [\Psi_1^{\dagger}(\mathbf{k}) \Psi_1(\mathbf{k}) + \Psi_2^{\dagger}(\mathbf{k}) \Psi_2(\mathbf{k})]. \quad (4.43)$$

Since Ψ_1 and Ψ_2 are free fields, the ground state is given by solving

$$\Psi_1(\mathbf{k}) |\Phi_{\text{exc}}\rangle = \Psi_2(\mathbf{k}) |\Phi_{\text{exc}}\rangle = 0, \quad (4.44)$$

or

$$|\Phi_{\text{exc}}\rangle = \prod_{\mathbf{k}} \frac{1}{\sqrt{2}} [1 + \psi_{\text{h}}^{\dagger}(\mathbf{k}) \psi_{\text{e}}^{\dagger}(\mathbf{k})] |0\rangle. \quad (4.45)$$

This is a BCS-type state representing the condensation of electron-hole pairs.

Due to the Fermi statistics the thermodynamical average $\langle \Psi_i^{\dagger}(\mathbf{k}) \Psi_j(\mathbf{k}) \rangle$ is given by

$$\begin{aligned} \langle \Psi_1^{\dagger}(\mathbf{k}) \Psi_1(\mathbf{k}) \rangle &= \langle \Psi_2^{\dagger}(\mathbf{k}) \Psi_2(\mathbf{k}) \rangle = \frac{1}{1 + e^{\Delta(\mathbf{k})/k_{\text{B}}T}}, \\ \langle \Psi_2^{\dagger}(\mathbf{k}) \Psi_1(\mathbf{k}) \rangle &= \langle \Psi_1^{\dagger}(\mathbf{k}) \Psi_2(\mathbf{k}) \rangle = 0, \end{aligned} \quad (4.46)$$

where k_{B} is the Boltzmann factor. Combining these with (4.42) we obtain

$$\langle \psi_{\text{e}}^{\dagger}(\mathbf{k}) \psi_{\text{h}}^{\dagger}(\mathbf{k}) \rangle = \frac{1}{2} \tanh \frac{\Delta(\mathbf{k})}{2k_{\text{B}}T}. \quad (4.47)$$

Substituting this into (4.40) we derive the gap equation,

$$\Delta(\mathbf{k}) = \frac{1}{2} \int d^2\mathbf{k}' V^{\text{eff}}(\mathbf{k}' - \mathbf{k}) \tanh \frac{\Delta(\mathbf{k}')}{2k_{\text{B}}T}. \quad (4.48)$$

In the limit $T \rightarrow 0$, the zero-momentum gap $\Delta(\mathbf{k})$ is given by the dispersionless relation

$$\Delta(\mathbf{k})|_{T=0} = \pi \sqrt{\frac{\pi}{2}} \frac{e^2}{4\pi\epsilon\ell_B} \equiv \Delta_0. \quad (4.49)$$

For finite temperature, assuming the gap is dispersionless, we obtain the relation

$$\frac{\Delta_T}{\Delta_0} = \tanh \frac{\Delta_T}{2k_{\text{B}}T}. \quad (4.50)$$

The critical temperature T_{C} at which $\Delta_T = 0$ is solved as $T_{\text{C}} = \Delta_0/2k_{\text{B}}$.

According to the diagonalized Hamiltonian (4.43), the excitonic condensation provides them with the mass Δ_0 , resolving the electron-hole degeneracy in the zero-energy state. Combining the results at the K and K' points, the 4-fold degenerate levels split into two 2-fold degenerate levels [Fig.5(d)] with the gap energy (4.49). This leads to a new plateau at $\nu = 0$, as illustrated in Fig.6

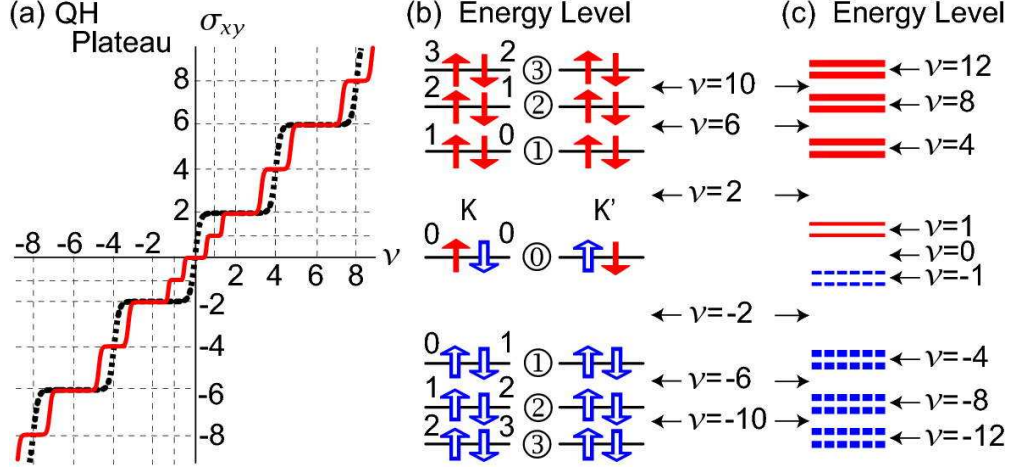


FIG. 6: (Color online) (a) The QH conductivity in graphene. The dotted black curve shows the sequence $\nu = \pm 2, \pm 6, \pm 10, \dots$, while the solid red curve the sequence $\nu = 0, \pm 1, \pm 2, \pm 4, \pm 6, \pm 8, \dots$. (b) The energy level within noninteracting theory, indicated by the number in circle. The spin is indicated by a solid red (open blue) arrow for electron (hole) at the K and K' points. The number attached to a solid red (open blue) arrow shows from which Landau level the electron (hole) comes from. (c) When Coulomb interactions are included, the zero-energy level splits into four nondegenerate subbands, while each nonzero-energy level splits into two 2-fold degenerate subbands with the exact U(1) symmetry.

V. VALLEY POLARIZATION

It is now possible to treat electrons and holes separately since the gap has opened between the electron and hole bands. Furthermore, it is enough to study only electrons due to the electron-hole symmetry. We show that the Coulomb effect modifies the energy spectrum of the noninteracting theory so that plateaux emerges at $\nu = \pm 1, \pm 2n$ with $n = 1, 2, 3, \dots$ [Fig.6].

We express the Coulomb Hamiltonian (3.32) as

$$H_N = \sum V_{N;mnij}^{\sigma\sigma';\tau\tau'\lambda\lambda'} c_{\tau}^{\sigma\dagger}(m) c_{\tau'}^{\sigma'}(n) c_{\lambda}^{\sigma'\dagger}(i) c_{\lambda'}^{\sigma'}(j), \quad (5.1)$$

where the summations over repeated indices, $m, n, i, j, \sigma, \sigma', \tau, \tau', \lambda, \lambda'$ are understood, and

$$V_{N;mnij}^{\sigma\sigma';\tau\tau'\lambda\lambda'} = \frac{1}{4\pi} \int d^2q V(\mathbf{q}) F_{\tau\tau'}^{\sigma}(-\mathbf{q}) F_{\lambda\lambda'}^{\sigma'}(\mathbf{q}) \times \langle m | e^{-i[\mathbf{q} + \tau\mathbf{K} - \tau'\mathbf{K}]\mathbf{X}} | n \rangle \langle i | e^{-i[\mathbf{q} + \lambda\mathbf{K} - \lambda'\mathbf{K}]\mathbf{X}} | j \rangle. \quad (5.2)$$

We introduce

$$V_{N;D}^{\tau\tau'\lambda\lambda'} = \sum_{ij} V_{N;ijjj}^{\uparrow\uparrow;\tau\tau'\lambda\lambda'}, \quad V_{N;X}^{\tau\tau'\lambda\lambda'} = \sum_{ij} V_{N;ijji}^{\uparrow\uparrow;\tau\tau'\lambda\lambda'}. \quad (5.3)$$

They represent the direct and exchange Coulomb energies, respectively. It is easy to evaluate them numerically: See Fig.7(a) for $V_{N;X}^{++++}$. We analyze the lowest energy level and higher energy levels separately.

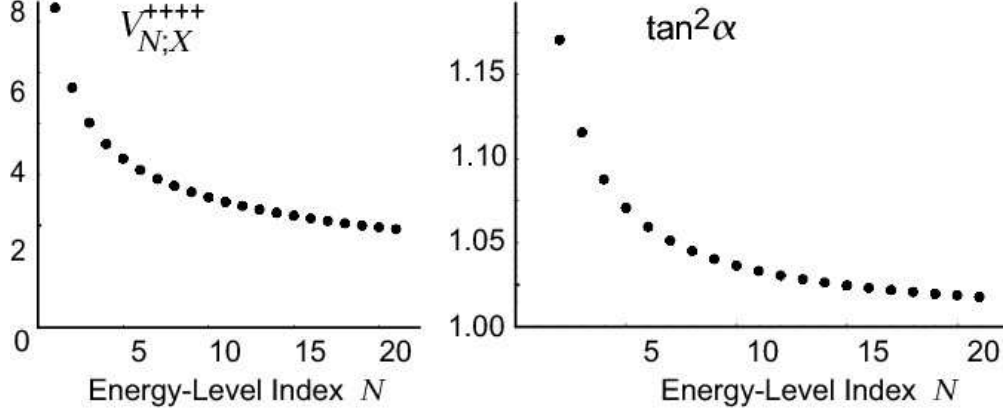


FIG. 7: (a) The exchange energy $V_{N;X}^{++++}$ of the N th energy level as a function of N . The vertical axis is the energy in unit of $e^2/4\pi\epsilon\ell_B$. Note that $V_{N;X}^{----} = V_{N-1;X}^{++++}$. (b) The function $\tan^2 \alpha_N$ given by (5.12). It approaches 1 asymptotically, $\lim_{N \rightarrow \infty} \tan^2 \alpha_N = 1$.

A. Lowest Energy Level

We first study the lowest energy level, which contain two degenerate states [Fig.6(b)]. The degeneracy is resolved obviously by a strong extrinsic Zeeman effect if it exists. We consider the case where the extrinsic Zeeman energy is absent at temperature $T = 0$, or is present but quite small compared with the thermal energy at $T \neq 0$. We ask whether the degeneracy is resolved even in such cases.

As a generic trial function we take

$$|\Phi_0\rangle = \prod_n \left(u c_+^{\dagger}(n) + v c_-^{\dagger}(n) \right) |0\rangle, \quad (5.4)$$

with $|u|^2 + |v|^2 = 1$. The state covers the entire $SU(2)$ space of the lowest energy level for electrons, when the two parameters u and v are varied.

We calculate the Coulomb energy $\langle H \rangle_0 \equiv \langle \Phi_0 | H | \Phi_0 \rangle$ with (5.1). Most terms are $SU(2)$ invariant, but there exists a noninvariant term,

$$\langle H_{\text{noninv}} \rangle_0 = 2\pi |uv|^2 V_{0;X}^{++++}. \quad (5.5)$$

Hence the $SU(2)$ symmetry is broken explicitly into the $U(1)$ symmetry by Coulomb interactions.

The energy is minimized either $u = 0$ or $v = 0$ due to the term (5.5), corresponding to the state

$$|\Phi_0^{\downarrow}\rangle = \prod_n c_-^{\dagger}(n) |0\rangle \quad \text{or} \quad |\Phi_0^{\uparrow}\rangle = \prod_n c_+^{\dagger}(n) |0\rangle. \quad (5.6)$$

The ground state is either $|\Phi_0^{\downarrow}\rangle$ or $|\Phi_0^{\uparrow}\rangle$, though there exists still the Z_2 symmetry. The energy barrier is of the order of the Coulomb energy, which is much larger than the thermal energy.

We conclude as follows: The two levels split explicitly by an extrinsic Zeeman effect if exists. Then the first energy level is up-spin polarized, and the second energy level is down-spin polarized. Even without such an extrinsic Zeeman effect, driven by the Coulomb exchange interaction, the spontaneous breakdown of the Z_2 symmetry turns the system into a QH ferromagnet^{26,27}. It is reasonable to call it the Ising QH ferromagnet due to the Z_2 symmetry. In any case, a plateau emerges at $\nu = 1$, where the activation energy is of the order of the typical Coulomb energy as in the conventional QHE^{26,27}.

B. N th Energy Level

We next study the N th energy level with $N \geq 1$. It contains four degenerate states with the $SU(4)$ symmetry in noninteracting theory. However, the projected density is invariant only under $U(1) \times U(1) \times Z_2$. Hence we take a set of trial functions by requiring this symmetry,

$$|\Phi_N^\uparrow\rangle = \prod_n \left(\sin \alpha_N e^{i\theta^\uparrow} c_+^{\uparrow\dagger}(n) + \cos \alpha_N e^{-i\theta^\uparrow} c_-^{\uparrow\dagger}(n) \right) |0\rangle, \quad (5.7a)$$

$$|\Phi_N^\downarrow\rangle = \prod_n \left(\cos \alpha_N e^{-i\theta^\downarrow} c_+^{\downarrow\dagger}(n) + \sin \alpha_N e^{i\theta^\downarrow} c_-^{\downarrow\dagger}(n) \right) |0\rangle, \quad (5.7b)$$

where the phase factors $e^{i\theta^\uparrow}$ and $e^{i\theta^\downarrow}$ assure the $U(1) \times U(1)$ symmetry. These two states are degenerate, $\langle \Phi_N^\uparrow | H_N | \Phi_N^\uparrow \rangle = \langle \Phi_N^\downarrow | H_N | \Phi_N^\downarrow \rangle$, due to the Z_2 symmetry.

It is easy to determine the angle α_N by minimizing the Coulomb energy $\langle \Phi_N^\sigma | H_N | \Phi_N^\sigma \rangle$. After some calculations we find

$$\langle \Phi_N^\uparrow | H_N | \Phi_N^\uparrow \rangle = A |\sin \alpha_N|^4 + B |\cos \alpha_N|^4 + C |\sin \alpha_N \cos \alpha_N|^2, \quad (5.8)$$

where

$$A = V_{N;D}^{++++} - V_{N;X}^{++++}, \quad B = V_{N;D}^{----} - V_{N;X}^{----}, \quad (5.9a)$$

$$C = V_{N;D}^{++--} + V_{N;D}^{--++} - V_{N;X}^{++--} - V_{N;X}^{--++} \quad (5.9b)$$

with (5.3). Here, $V_{N;D}^{++++} = V_{N;D}^{----} = V_{N;D}^{++--} = V_{N;D}^{--++}$ since $F_{\tau\tau}^\sigma(0) = 1$. Furthermore, because of (3.31), $V_{N;X}^{++--}$ and $V_{N;X}^{--++}$ are exponentially smaller in $(a/\ell_B)^2$ than $V_{N;X}^{++++}$ or $V_{N;X}^{----}$, and can be neglected. Hence

$$\tan^2 \alpha_N = \frac{B - C/2}{A - C/2} \simeq \frac{V_{N;X}^{----}}{V_{N;X}^{++++}}. \quad (5.10)$$

Now it follows from (3.29) that $V_{N;X}^{----} = V_{N-1;X}^{++++}$. We can also see [Fig.7(a)]

$$V_{N-1;X}^{++++} > V_{N;X}^{++++}, \quad (5.11)$$

implying that the Coulomb energy of an electron in higher Landau level is lower. It follows that

$$\tan^2 \alpha_N \simeq \frac{V_{N-1;X}^{++++}}{V_{N;X}^{++++}} > 1. \quad (5.12)$$

We have depicted $\tan^2 \alpha_N$ as a function of N in Fig.7(b).

We conclude that, if we take the state $|\Phi_N^\uparrow\rangle$, more electrons are present in the Dirac valley at the K point than at the K' point since $|\sin \alpha_N| > |\cos \alpha_N|$. Namely, the valley polarization has occurred both in $|\Phi_N^\uparrow\rangle$ and $|\Phi_N^\downarrow\rangle$. This can be understood physically as follows [Fig.1(a)]: Up-spin electrons in the K point belong to the $(N-1)$ th Landau level but those in the K' point belong to the N th Landau level. It is easier to fill Landau sites at the K point because the Coulomb energy is lower in higher Landau levels. The valley polarization disappears as $N \rightarrow \infty$, since $V_{N+1;X}^{----} = V_{N;X}^{----}$ in the limit [Fig.7(b)].

An extrinsic Zeeman effect open a gap between these two spin polarized states. Even without such an effect, driven by the Coulomb exchange interaction, the spontaneous breakdown of the Z_2 symmetry turns the system into a QH ferromagnet. Note that it has still the 2-fold degeneracy. In any case, a plateau emerges at $\nu = 4N$ [Fig.6(c)], where the activation energy is of the order of the typical Coulomb energy as in the conventional QHE^{26,27}.

VI. MULTILAYER GRAPHENE SYSTEMS

A. Bilayer Graphene (Bernal Stacking)

We proceed to generalize the above analysis to a bilayer graphene, which is a system made of two coupled hexagonal lattices according to the Bernal stacking. In the absence of magnetic field, the low-energy spectrum of the bilayer graphene is known^{4,15,16,35} to be parabolic,

$$\mathcal{E}(k) \propto |\mathbf{k}|^2, \quad (6.1)$$

near the K and K' points. In the presence of the magnetic field, we can reformulate the model Hamiltonian^{15,16,35} as the generalized Dirac Hamiltonian defined by

$$H^\pm = \text{diag.} \left(\sqrt{Q_\pm Q_\pm}, -\sqrt{Q_\pm Q_\pm} \right), \quad (6.2)$$

together with

$$Q_+ = \begin{pmatrix} 0 & A^\dagger \\ A & 0 \end{pmatrix}, \quad Q_- = \begin{pmatrix} 0 & A \\ A^\dagger & 0 \end{pmatrix}. \quad (6.3)$$

Here, $A = \hbar\omega_c a^2$, with a given by (2.14). We also consider the generalized Pauli Hamiltonian

$$H_P^+ \equiv Q_+ Q_+ = (\hbar\omega_c)^2 \begin{pmatrix} a^{2\dagger} a^2 & 0 \\ 0 & a^2 a^{2\dagger} \end{pmatrix}, \quad (6.4a)$$

$$H_P^- \equiv Q_- Q_- = (\hbar\omega_c)^2 \begin{pmatrix} a^2 a^{2\dagger} & 0 \\ 0 & a^{2\dagger} a^2 \end{pmatrix}. \quad (6.4b)$$

We may switch off the magnetic field in this formula, and reproduce the energy spectrum (6.1).

The eigenvalue of the Hamiltonian H^\pm is derived as

$$H^\pm |N\rangle = \left(\mathcal{E}_N^{\pm\dagger}, \mathcal{E}_N^{\pm\downarrow}, -\mathcal{E}_N^{\pm\dagger}, -\mathcal{E}_N^{\pm\downarrow} \right) |N\rangle \quad (6.5)$$

with the eigenstate $|N\rangle = (N!)^{-1/2} (a^\dagger)^N |0\rangle$, where

$$\mathcal{E}_N^{+\dagger} = \mathcal{E}_N^{-\downarrow} = \hbar\omega_c \sqrt{N(N-1)}, \quad (6.6a)$$

$$\mathcal{E}_N^{+\downarrow} = \mathcal{E}_N^{-\dagger} = \hbar\omega_c \sqrt{(N+2)(N+1)} \quad (6.6b)$$

for $N = 0, 1, 2, 3$, as illustrated in Fig.8. It is interesting that two Landau levels mix to create one nonzero-energy level, but that four Landau levels mix to create the zero-energy level. Thus there exists the 4-fold degeneracy in the nonzero-energy level but the 8-fold degeneracy in the zero-energy state, as results in the bold-face series (1.2). This agrees with the previous result^{4,15,16}.

We include Coulomb interactions. The N th energy level ($N \neq 0$) has the same structure as in the monolayer graphene system. Coulomb interactions make each energy level split into two subbands.

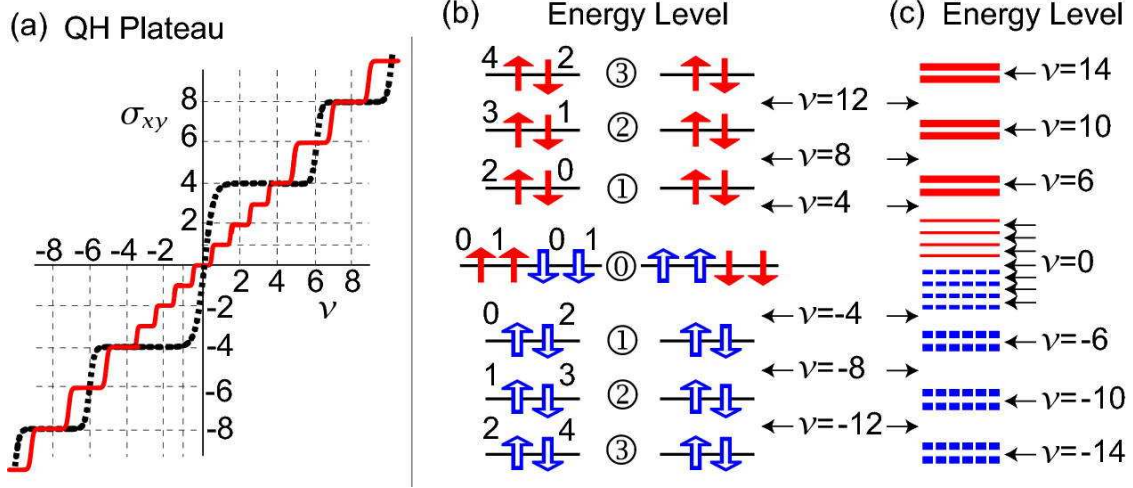


FIG. 8: (Color online) (a) The QH conductivity in bilayer graphene. The dotted black curve shows the sequence $\nu = \pm 4, \pm 8, \pm 12, \dots$, while the solid red curve the sequence $\nu = 0, \pm 1, \pm 2, \pm 3, \pm 4, \pm 6, \pm 8, \dots$. (b) The energy level within noninteracting theory. The spin is indicated by a solid red (open blue) arrow for electron (hole) at the K and K' points. The number attached to a solid red (open blue) arrow shows from which Landau level the electron (hole) comes from. (c) When Coulomb interactions are included, the zero-energy level splits into eight nondegenerate subbands, while each nonzero-energy level splits into two 2-fold degenerate subbands with the exact U(1) symmetry.

We discuss the zero-energy state in some details. There are electron-hole pairs coming from the $N = 0$ Landau level and the $N = 1$ Landau level for electrons and holes [Fig.8(b)]. At the K point there are four gap functions $\Delta_{00}(\mathbf{k})$, $\Delta_{11}(\mathbf{k})$, $\Delta_{01}(\mathbf{k})$ and $\Delta_{10}(\mathbf{k})$,

$$\Delta_{NN'}(\mathbf{k}) = \int d^2k' V^{\text{eff}}(\mathbf{k}' - \mathbf{k}) \langle \psi_e^{N\uparrow\dagger}(\mathbf{k}') \psi_h^{N'\downarrow\dagger}(\mathbf{k}') \rangle, \quad (6.7)$$

where $\psi_e^{N\uparrow\dagger}$ and $\psi_h^{N'\downarrow\dagger}$ are creation operators of electrons in the N th Landau level and holes in the N' th Landau level, respectively. Repeating similar analysis we have made in Section IV, we solve the gap equations at $T = 0$ as

$$\Delta_{00}(\mathbf{k}) = \Delta_0, \quad (6.8a)$$

$$\Delta_{11}(\mathbf{k}) = \frac{3}{4}\Delta_0, \quad (6.8b)$$

$$\Delta_{01}(\mathbf{k}) = \Delta_{10}(\mathbf{k}) = \frac{1}{2}\Delta_0, \quad (6.8c)$$

where Δ_0 is given by (4.49); $\Delta_0 = \pi\sqrt{\pi/2}(e^2/4\pi\epsilon\ell_B)$. Thus, the 8-fold degenerate zero-energy level splits into four 2-fold degenerated subbands, producing plateaux at $\nu = \pm 2, \pm 4$. Furthermore we have Ising QH ferromagnets at $\nu = \pm 1, \pm 3$. Consequently, we predict the full series (1.2).

B. Trilayer Graphene (Rhombohedral Stacking)

The above analysis is applicable also to a trilayer graphene with the ABC stacking (rhombohedral stacking). In the absence of the magnetic field, the low-energy spectrum of trilayer graphene has

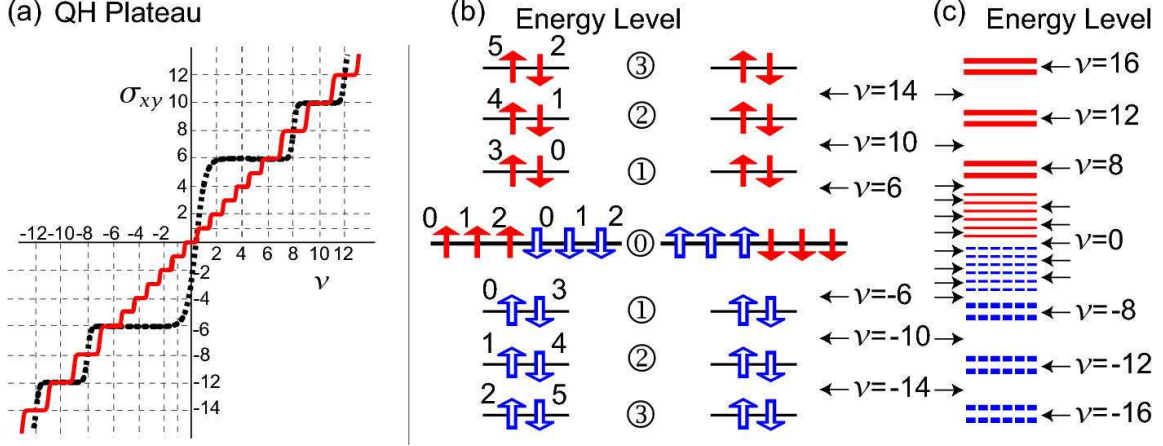


FIG. 9: (Color online) (a) The QH conductivity in trilayer graphene. The dotted black curve shows the sequence $\nu = \pm 6, \pm 10, \pm 14, \dots$, while the solid red curve the sequence $\nu = 0, \pm 1, \pm 2, \pm 3, \pm 4, \pm 5, \pm 6, \pm 8, \pm 10, \dots$. (b) The energy level within noninteracting theory. The spin is indicated by a solid red (open blue) arrow for electron (hole) at the K and K' points. The number attached to a solid red (open blue) arrow shows from which Landau level the electron (hole) comes from. (c) When Coulomb interactions are included, the zero-energy level splits into twelve nondegenerate subbands, while each nonzero-energy level splits into two 2-fold degenerate subbands with the exact U(1) symmetry.

been argued¹⁶ to be cubic,

$$\mathcal{E}(k) \propto |\mathbf{k}|^3, \quad (6.9)$$

near the K and K' points. In the presence of the magnetic field, we can reformulate the model Hamiltonian¹⁶ as the generalized Dirac Hamiltonian as

$$H^\pm = \text{diag.} \left(\sqrt{Q_\pm Q_\pm}, -\sqrt{Q_\pm Q_\pm} \right), \quad (6.10)$$

together with

$$Q_+ = \begin{pmatrix} 0 & A^\dagger \\ A & 0 \end{pmatrix}, \quad Q_- = \begin{pmatrix} 0 & A \\ A^\dagger & 0 \end{pmatrix}. \quad (6.11)$$

Here, $A = \hbar\omega_c a^3$, where a given by (2.14).

The eigenvalue of the Hamiltonian H^\pm is derived as in (6.5) with

$$\mathcal{E}_N^{+\uparrow} = \mathcal{E}_N^{-\downarrow} = \hbar\omega_c \sqrt{N(N-1)(N-2)}, \quad (6.12a)$$

$$\mathcal{E}_N^{+\downarrow} = \mathcal{E}_N^{-\uparrow} = \hbar\omega_c \sqrt{(N+3)(N+2)(N+1)} \quad (6.12b)$$

for $N = 0, 1, 2, 3$, as illustrated in Fig.8. There exists the 4-fold degeneracy in the nonzero-energy level but the 12-fold degeneracy in the zero-energy state, as results in the bold-face series (1.3). This agrees with the previous result¹⁶.

We briefly argue how the energy spectrum is modified by Coulomb interactions. The effective Coulomb potential depends on the spin and the valley degree of freedom precisely by the same mechanism. The N th energy level ($N \neq 0$) has the same structure as in the monolayer graphene

system. Hence, each energy level splits into two subbands. The ground state is describe by a formula similar to (5.7), where the valley polarization is occurred. There are electron-hole pairs in the zero-energy state, which make excitonic condensation by the same mechanism as in the monolayer and bilayer cases. Thus, the 12-fold degenerate zero-energy level splits into six 2-fold degenerated subbands, producing plateaux at $\nu = \pm 2, \pm 4, \pm 6$. Furthermore we have Ising QH ferromagnets at $\nu = \pm 1, \pm 3, \pm 5$. Consequently, we predict the full series (1.3).

VII. DISCUSSIONS

The most intriguing property of the graphene system is that the intrinsic Zeeman energy is precisely one half of the cyclotron energy for electrons and holes. It leads to the symmetry group SU(4) in the noninteracting theory, where the Hall plateau emerges at $\nu = \pm 2, \pm 6, \pm 10, \dots$. This series is the first experimental result² of the QHE in graphene. When Coulomb interactions are included, the symmetry SU(4) is broken so that the Hall plateau emerges at $\nu = 0, \pm 1, \pm 4, \pm 8, \dots$. This series has been found experimentally⁵ when larger magnetic field is applied. We have shown that the Ising QH ferromagnets appear at $\nu = \pm 1$ due to a BCS-type condensation of electron-hole pairs.

We have emphasized that one energy level contains up-spin and down-spin electrons coming from two neighboring Landau levels. Since Coulomb interactions are different for electrons in different Landau levels, we have derived a remarkable consequence that the effective Coulomb potential depends on the spin and the valley degree of freedom [Figs.3 and 4]. As a result, the valley polarization is occurred on the ground state. We wish to explore new physics associated with this peculiar Coulomb interaction in forthcoming papers.

Acknowledgement

The work was in part supported by Grants-in-Aid for Scientific Research from Ministry of Education, Science, Sports and Culture (Nos.070500000466).

APPENDIX A: DIRAC ELECTRONS IN GRAPHENE

In this appendix, we derive the second-quantized Dirac Hamiltonian (2.3) together with (2.4) for electrons in graphene. We start with a study on the quantum-mechanical states of electrons based on the $\mathbf{k} \cdot \mathbf{p}$ approximation^{17,19}.

First of all, the wave functions $f_S^\tau(\mathbf{x})$ are given in terms of envelope functions $F_S^\tau(\mathbf{x})$ as²¹

$$f_S^K(\mathbf{x}) = e^{i\mathbf{K} \cdot \mathbf{x}} F_S^K(\mathbf{x}), \quad f_S^{K'}(\mathbf{x}) = e^{-i\mathbf{K} \cdot \mathbf{x}} F_S^{K'}(\mathbf{x}), \quad (1.13)$$

where S is the site index ($S = A, B$) and τ is the valley index ($\tau = K, K'$). The envelope functions are normalized as $|F_S^K(\mathbf{x})|^2 + |F_S^{K'}(\mathbf{x})|^2 = 1/2$ for $S = A, B$. They satisfy the Schrödinger equation²¹

$$H_0 \mathbf{F}(\mathbf{x}) = \mathcal{E} \mathbf{F}(\mathbf{x}), \quad (1.14)$$

where \mathcal{E} is the eigenvalue, and the Hamiltonian H_0 is the 4×4 matrix operator,

$$H_0 = v_F \begin{pmatrix} 0 & p_x - ip_y & 0 & 0 \\ p_x + ip_y & 0 & 0 & 0 \\ 0 & 0 & 0 & p_x + ip_y \\ 0 & 0 & p_x - ip_y & 0 \end{pmatrix}, \quad (1.15)$$

with $p_k = -i\hbar\partial_k$. Since this is block diagonal, it is convenient to set

$$H_R^K = v_F(\boldsymbol{\sigma} \cdot \mathbf{p}) = v_F \begin{pmatrix} 0 & p_x - ip_y \\ p_x + ip_y & 0 \end{pmatrix}, \quad (1.16a)$$

$$H_R^{K'} = v_F(\boldsymbol{\sigma} \cdot \mathbf{p}') = \begin{pmatrix} 0 & p_x + ip_y \\ p_x - ip_y & 0 \end{pmatrix}, \quad (1.16b)$$

with $\mathbf{p}' = (p_x, -p_y)$. Note that $H_R^{K'} = \sigma_x H_R^K \sigma_x$, where σ_x is the generator of the mirror symmetry. The eigenfunctions of H_R^τ ($\tau = K, K'$) are given by²¹

$$\mathbf{F}_\sigma^{\tau;R}(\mathbf{x}) = \begin{pmatrix} F_A^\tau(\mathbf{x}) \\ \sigma F_B^\tau(\mathbf{x}) \end{pmatrix}, \quad (1.17)$$

with the eigenvalue $\mathcal{E}(\mathbf{k}') = \sigma \hbar v_F |\mathbf{k}'|$, where σ stands for the helicity, $\sigma = \pm$. Note that $\hbar \mathbf{k}'$ is the momentum of electrons, $|\mathbf{k}'| \ll |\mathbf{K}|$ measured from the K or K' point.

Let us explain the notations we have used in (1.16) and (1.17). We recall that the $\boldsymbol{\sigma} \cdot \mathbf{p}$ is the helicity operator except for the positive normalization factor. Thus, $\mathbf{F}_+^{K;R}(\mathbf{x})$ has the positive helicity and a positive energy, while $\mathbf{F}_-^{K;R}(\mathbf{x})$ has the negative helicity and a negative energy. Since the energy and the helicity have the same sign for the envelope function $\mathbf{F}_\sigma^{K;R}(\mathbf{x})$, it describes the right-handed Weyl fermion by definition. Hence we have put the index "R". Similarly we have assigned the right-handed Weyl fermion at the K' point.

There are only four independent two-component envelope functions given by (1.17) with $\tau = K, K'$ and $\sigma = \pm$. However, there are more quantum-mechanical states for electrons. They are the chiral symmetric copies; the left-handed Weyl fermions $\mathbf{F}_\sigma^{K;L}(\mathbf{x})$ at the K point and $\mathbf{F}_\sigma^{K';L}(\mathbf{x})$ at the K' point. The corresponding Hamiltonians and envelope functions are constructed by the chiral transformation generated by the Pauli matrix σ_z as $H_L^K = \sigma_z H_R^K \sigma_z = -v_F(\boldsymbol{\sigma} \cdot \mathbf{p})$, $H_L^{K'} = \sigma_z H_R^{K'} \sigma_z = -v_F(\boldsymbol{\sigma} \cdot \mathbf{p}')$, and

$$\mathbf{F}_\sigma^{\tau;L}(\mathbf{x}) = \sigma_z \mathbf{F}_\sigma^{\tau;R}(\mathbf{x}) = \begin{pmatrix} F_A^\tau(\mathbf{x}) \\ -\sigma F_B^\tau(\mathbf{x}) \end{pmatrix}. \quad (1.18)$$

Note the the energy and the helicity have the opposite sign for the left-handed Weyl fermion.

The energy spectrum is symmetric between the positive and negative energy states. There exists one electron per one carbon and the band-filling factor is 1/2 in graphene. Namely, all negative-energy states are filled up, as is a reminiscence of the Dirac sea. Hence, we have electrons and holes as physical excitations.

In this way there are eight types of quantum-mechanical states for electrons in graphene, corresponding to the spin degree of freedom ($\sigma = \pm$), the electron-hole degree of freedom and the

valley degree of freedom ($\tau = K, K'$). To carry out the second quantization it is necessary to use all these quantum-mechanical states together with the four Hamiltonians. We arrange them as $H_D^K = v_F \boldsymbol{\sigma} \cdot \mathbf{p} \gamma_5$, $H_D^{K'} = -v_F \boldsymbol{\sigma} \cdot \mathbf{p}' \gamma_5$ where we have introduced the Dirac γ_5 matrix in the Weyl representation,

$$\gamma_5 = \begin{pmatrix} 1 & 0 \\ 0 & -1 \end{pmatrix}. \quad (1.19)$$

They are summarized into the Dirac Hamiltonian (2.4) in text, or

$$H_D^\tau = v_F (\tau \sigma_x p_x + \sigma_y p_y) \gamma_5, \quad (1.20)$$

where $\tau = + (-)$ for the K (K') point.

According to the standard prescription the second-quantized Hamiltonian is constructed as in (2.3), or $H = \sum_{\tau=\pm} \int d^2x \Psi_\tau^\dagger(\mathbf{x}) H_D^\tau \Psi_\tau(\mathbf{x})$, where H_D^τ is the quantum mechanical Hamiltonian. The field operator is expanded as $\Psi_\tau(\mathbf{x}) = \Psi_{e\tau}(\mathbf{x}) + \Psi_{h\tau}(\mathbf{x})$, with

$$\Psi_{e\tau}(\mathbf{x}) = \sum_{\sigma=\pm} \int \frac{d^2k'}{2\pi} c_\tau^\sigma(\mathbf{k}') u_\sigma^\tau(\mathbf{k}') e^{i\mathbf{k}'\mathbf{x}}, \quad (1.21a)$$

$$\Psi_{h\tau}(\mathbf{x}) = \sum_{\sigma=\pm} \int \frac{d^2k'}{2\pi} d_\tau^{\sigma\dagger}(\mathbf{k}') v_\sigma^\tau(\mathbf{k}') e^{-i\mathbf{k}'\mathbf{x}}. \quad (1.21b)$$

We have introduced the annihilation operator $c_\tau^\sigma(\mathbf{k}')$ of an electron with the eigenfunction $u_\sigma^\tau(\mathbf{k}')$, and the creation operator $d_\tau^{\sigma\dagger}(\mathbf{k}')$ of a hole with the eigenfunction $v_\sigma^\tau(\mathbf{k}')$, where we have set $u_+^\tau(\mathbf{k}') = \mathbf{F}_+^{\tau;R}(\mathbf{k}')$, $u_-^\tau(\mathbf{k}') = \mathbf{F}_-^{\tau;L}(\mathbf{k}')$, $v_+^\tau(\mathbf{k}') = \mathbf{F}_+^{\tau;L}(-\mathbf{k}')$ and $v_-^\tau(\mathbf{k}') = \mathbf{F}_-^{\tau;R}(-\mathbf{k}')$ in accord with the standard notation in the Dirac theory. In passing, the field operator $\psi_\tau(\mathbf{x})$ for electrons in graphene is to be constructed with the use of the wavefunction (1.13), and hence is given by (2.7) in text.

II. LANDAU-LEVEL PROJECTION

In this appendix we derive the formula (3.27) for the projected density operator $\rho_N(\mathbf{q})$. We first review how the Landau-level projection is made in the conventional QHE, where the density operator is given by $\rho(\mathbf{x}) = \psi^\dagger(\mathbf{x})\psi(\mathbf{x})$. We consider electrons confined to the N th Landau level, where Fock states are given by (2.22). The field operator is expanded as

$$\psi(\mathbf{x}) = \sum_n \langle \mathbf{x} | N, n \rangle c(n), \quad (2.22)$$

with $c(n)$ the annihilation operator of electrons acting on the state $|N, n\rangle$, $\{c(n), c^\dagger(m)\} = \delta_{nm}$. The projected density operator is

$$\rho_N(\mathbf{x}) = \psi^\dagger(\mathbf{x})\psi(\mathbf{x}) = \sum_{mn} \langle N, m | \mathbf{x} \rangle \langle \mathbf{x} | N, n \rangle c^\dagger(m) c(n). \quad (2.23)$$

Its Fourier transformation is

$$\rho_N(\mathbf{q}) = \frac{1}{2\pi} \sum_{mn} \int d^2x e^{-i\mathbf{q}\mathbf{x}} \langle N, m | \mathbf{x} \rangle \langle \mathbf{x} | N, n \rangle c^\dagger(m) c(n). \quad (2.24)$$

Here, we decompose the coordinate into the guiding center and the relative coordinate, $\mathbf{x} = \mathbf{X} + \mathbf{R}$, where \mathbf{X} and \mathbf{R} act on the Fock states $|n\rangle$ and $|N\rangle$, respectively. Since they commute each other, we obtain

$$\rho_N(\mathbf{q}) = \frac{1}{2\pi} \sum_{mn} \langle N | e^{-i\mathbf{q}\mathbf{R}} | N \rangle \langle m | e^{-i\mathbf{q}\mathbf{X}} | n \rangle c^\dagger(m) c(n), \quad (2.25)$$

or $\rho_N(\mathbf{q}) = F_N(\mathbf{q}) \hat{\rho}(\mathbf{q})$, with

$$F_N(\mathbf{q}) = \langle N | e^{-i\mathbf{q}\mathbf{R}} | N \rangle, \quad (2.26a)$$

$$\hat{\rho}(\mathbf{q}) = \frac{1}{2\pi} \sum_{mn} \langle m | e^{-i\mathbf{q}\mathbf{X}} | n \rangle c^\dagger(m) c(n). \quad (2.26b)$$

We call $F_N(\mathbf{q})$ the Landau-level form factor, and $\hat{\rho}(\mathbf{q})$ the bare density operator.

In the graphene QHE one energy level contain four different types of electrons described by (2.23). For instance, the projected density operator for up-spin electrons is given by

$$\begin{aligned} \rho_N^\uparrow(\mathbf{x}) = & \langle N, m | \mathbf{x} \rangle \langle \mathbf{x} | N, n \rangle c_+^{\dagger\dagger}(m) c_+^\dagger(n) + \langle N-1, m | \mathbf{x} \rangle \langle \mathbf{x} | N-1, n \rangle c_-^{\dagger\dagger}(m) c_-^\dagger(n) \\ & + e^{-2i\mathbf{K}\mathbf{x}} \langle N, m | \mathbf{x} \rangle \langle \mathbf{x} | N-1, n \rangle c_+^{\dagger\dagger}(m) c_-^\dagger(n) + e^{2i\mathbf{K}\mathbf{x}} \langle N-1, m | \mathbf{x} \rangle \langle \mathbf{x} | N, n \rangle c_-^{\dagger\dagger}(m) c_+^\dagger(n), \end{aligned}$$

where the summation over the indices n and m is understood. By repeating the above process, this reads

$$\begin{aligned} \rho_N^\uparrow(\mathbf{q}) = & F_{N,N}^{++}(\mathbf{q}) \hat{D}_{++}^{\uparrow\uparrow}(\mathbf{q}) + F_{N-1,N-1}^{--}(\mathbf{q}) \hat{D}_{--}^{\uparrow\uparrow}(\mathbf{q}) \\ & + F_{N,N-1}^{+-}(\mathbf{q}) \hat{D}_{+-}^{\uparrow\uparrow}(\mathbf{q}) + F_{N-1,N}^{-+}(\mathbf{q}) \hat{D}_{-+}^{\uparrow\uparrow}(\mathbf{q}), \end{aligned} \quad (2.27)$$

where

$$F_{N,M}^{\tau\tau'}(\mathbf{q}) = \langle N | e^{-i[\mathbf{q} + \tau\mathbf{K} - \tau'\mathbf{K}]\mathbf{R}} | M \rangle, \quad (2.28)$$

and

$$\hat{D}_{\tau\tau'}^{\sigma\sigma'}(\mathbf{q}) = \frac{1}{2\pi} \sum_{mn} \langle m | e^{-i[\mathbf{q} + \tau\mathbf{K} - \tau'\mathbf{K}]\mathbf{X}} | n \rangle c_\tau^{\sigma\dagger}(n) c_{\tau'}^{\sigma'}(m). \quad (2.29)$$

A similarly formula is derived also for $\rho_N^\downarrow(\mathbf{q})$. Adding $\rho_N^\uparrow(\mathbf{q})$ and $\rho_N^\downarrow(\mathbf{q})$ we obtain (3.27) in text.

¹ K.S. Novoselov, A.K. Geim, S.V. Morozov, D. Jiang, Y. Zhang, S.V. Dubonos, I.V. Grigorieva, and A.A. Firsov, Science **306**, 666 (2004).

² K.S. Novoselov, A.K. Geim, S.V. Morozov, D. Jiang, M.I. Katsnelson, I.V. Grigorieva, S.V. Dubonos and A.A. Firsov, Nature **438**, 197 (2005).

³ Y. Zhang, Yan-Wen Tan, Horst L. Stormer and Philip Kim, Nature **438**, 201 (2005).

⁴ K.S. Novoselov, E. McCann, S. V. Morozov, V.I. Fal'ko, M.I. Katsnelson, U. Zeitler, D. Jiang, F. Schen-dini and A.K. Geim, Nature Phys. **2**, 177 (2006).

- ⁵ Y. Zhang Z. Jiang, J.P. Small, M.S. Purewal, Y.-W. Tan, M. Fazlollahi, J.D. Chudow, J.A. Jaszczak, H.L. Stormer, and P. Kim, Phys. Rev. Lett. **96**, 136806 (2006).
- ⁶ J.W. McClure, Phys. Rev. **104**, 666 (1956).
- ⁷ Y. Zheng and T. Ando, Phys. Rev. B **65**, 245420 (2002).
- ⁸ V.P. Gusynin and S.G. Sharapov, Phys. Rev. Lett. **95**, 146801 (2005).
- ⁹ N.M.R. Peres, F. Guinea and A.H.C. Neto, Phys. Rev. B **73**, 125411 (2006).
- ¹⁰ J. Alicea and M.P.A. Fisher, Phys. Rev. B **74**, 075422 (2006).
- ¹¹ K. Nomura and A.H. MacDonald, Phys. Rev. Lett. **96**, 256602 (2006).
- ¹² M. Goerbig, R. Moessner and B. Doucot, Phys. Rev. B **74**, 161407 (2006).
- ¹³ V.P. Gusynin, V.A. Miransky, S.G. Sharapov and I.A. Shovkovy, Phys. Rev. B **74**, 195429 (2006).
- ¹⁴ M. Ezawa, cond-mat/0606084; cond-mat/0609612.
- ¹⁵ E. McCann and V.I. Fal'ko., Phys. Rev. Lett. **96**, 086805 (2006).
- ¹⁶ F. Guinea, A.H. Castro Neto, and N.M.R. Peres, Phys. Rev. B **73**, 245426 (2006).
- ¹⁷ J.C. Slonczewski and P.R. Weiss, Phys. Rev. **109**, 272 (1958).
- ¹⁸ G. W. Semenoff, Phys. Rev. Lett. **53**, 2449 (1984).
- ¹⁹ H. Ajiki and T. Ando, J. Phys. Soc. Jpn., **62**, 1255 (1993); T. Ando, Y. Zheng and H. Suzuura, Micro-electronic Engineering, **63**, 167 (2002).
- ²⁰ S.Y. Zhou, G.-H. Gweon, J. Graf, A. V. Fedorov, C. D. Spataru, R. D. Diehl, Y. Kopelevich, D.-H. Lee, S.G. Louie, A. Lanzara, Nature Phys. **2**, 595 (2006).
- ²¹ T. Ando, J. Phys. Soc. Jpn., **74**, 777 (2005).
- ²² R.P. Feynman and M. Gell-Mann, Phys. Rev. **109**, 193 (1958).
- ²³ E. Witten, Nucl. Phys. B **185**, 513 (1981); Nucl. Phys. B **202**, 253 (1982).
- ²⁴ B. Thaller, *The Dirac Equation* (Springer-Verlag, Berlin, 1992).
- ²⁵ R.E. Prange and S.M. Girvin (eds), *The Quantum Hall Effect* (Springer, 1990) 2nd ed..
- ²⁶ S. Das Sarma and A. Pinczuk (eds), *Perspectives in Quantum Hall Effects* (Wiley, 1997).
- ²⁷ Z.F. Ezawa, *Quantum Hall Effects* (World Scientific, 2000).
- ²⁸ S.M. Girvin and T. Jach, Phys. Rev. B **29**, 5617 (1984).
- ²⁹ Z.F. Ezawa and G. Tsitsishvili, Phys. Rev. D **72**, 85002 (2005).
- ³⁰ T. Ando and Y. Uemura, J. Phys. Soc. Jpn. **37**, 1044 (1974).
- ³¹ N. Shibata and D. Yoshioka, J. Phys. Soc. Jpn. **73**, (2004) 2169.
- ³² D. V. Khveschenko, Phys. Rev. Lett. **87**, 206401 (2001).
- ³³ D. V. Khveschenko, Phys. Rev. Lett. **87**, 246802 (2001).
- ³⁴ E. Gorbar, V. Gusynin, V. Miransky, and I. Shovkovy, Phys. Rev. B **66**, 045108 (2002).
- ³⁵ M. Koshino and T. Ando, Phys. Rev. B **73**, 245403 (2006).